Supporting Information for

The effect of aging on the stability of microbially reduced uranium in natural sediments

Luca Loreggian[†], Agnes Novotny[†], Sophie Louise Bretagne[†], Barbora Bartova[†], Yuheng Wang[‡], and Rizlan Bernier-Latmani[,†]*

† Environmental Microbiology Laboratory (EML), EPFL-ENAC-IIE-EML, Ecole Polytechnique Federale de Lausanne (EPFL), Station 6, CH-1015 Lausanne, Switzerland

‡ Research Center for Ecology and Environmental Sciences, Northwestern Polytechnical University, Xi'an, P. R. China

Corresponding Author

*E-mail: rizlan.bernier-latmani@epfl.ch

This PDF file includes:

Description of sediments and RAGW

Methods for the characterization of the effluent composition

Methods for the elemental composition in the sediments by XRF and chemical extraction

Discussion of sulfur speciation based on linear combination fit on XANES at S K-edge

Method for scanning electron microscopy (STEM)

Supplementary Tables S1 to S10

Supplementary Figure S1 to S17

Equations S1 and S2

References

Number of pages: 21

Description of the sediments and RAGW

The sediments used in all experiments were from an undisturbed location in a former U mining and milling processing site in Old Rifle, CO (USA), in the Colorado River Basin, which is part of the Uranium Mill Tailings Remedial Action (UMTRA) program of the U.S. Department of Energy[1]. The sediments sampled at Old Rifle were designated as Rifle area background sediment (RABS)[2]. RABS were dried, sieved (<2 mm) and stored in the dark until use. At Old Rifle, groundwater is confined in the topmost layer by a relatively impermeable silty shale layer at ~6 m depth[1,3]. The groundwater flows towards the Colorado River at ~0.82 m/day [3]. The concentration of dissolved oxygen ranges from 0 to 0.6 mg/L, with an average of 0.2 mg/L[4]. The aqueous U concentration varies between 0.4 and 1.8 µM [5]. In general, the aquifer has a high concentration of sulfate (SO_4^{2-}) (9-16 mM)[6,7] and high alkalinity (~10 meq/L). In this study, Rifle artificial groundwater (RAGW) was prepared to mimic conditions in the field (SI Table S1). RAGW composition was designed based on Rifle groundwater composition measured in previous studies[5,7]. RAGW was prepared anoxically by purging the solution with CO_2/N_2 gas (20:80) in sealed glass bottles and autoclaved.

Characterization of the effluent composition

The column effluent was routinely sampled for analysis of its composition throughout the experiment. Water samples were filtered through 0.22 µm PTFE filters before analysis for total U, total Fe, and SO_4^{2-} concentration. Total U both in the influent and effluent was analyzed using inductively-coupled plasma mass spectrometry (ICP-MS; Perkin Elmer ELAN DRC II). Total Fe was measured in the effluents by inductively-coupled plasma optical emission spectrometry (ICP-OES; Multitype ICP Emission Spectrometer, ICPE-9000, Shimadzu). Fe(II) was preserved from rapid oxidation by collecting 0.5 mL of effluent solution directly into 0.5 mL of 1 N HCl. The concentration of Fe(II) was determined photometrically on filtered samples with the Ferrozine method[8]. Sulfate remaining in the effluent was analyzed with Ion Chromatography (IC) (System ICS-3000 Dionex).

Chemistry of the sediments (XRF)

The concentration of major and trace elements in the sediments was measured by X-ray fluorescence spectrometry with a PANalytical Axio-mAX spectrometer. Briefly, the analysis was conducted on dried and homogenized samples that were prepared by pressing a minimum of 4 g of powder with Hoechst-wax-C in disks. The limit of detection depends on the element, and it ranges between 1 and 7 ppm. The accuracy of the instrument was verified using standard reference materials

Chemical extraction of uranium

Quantitative speciation of U in bioreduced RABS was performed via anoxic bicarbonate extraction according to a protocol based on Alessi et al.[9]. The chemical extraction was conducted in an anoxic atmosphere (3%:97% H_2:N_2) in a glove box (Coy Laboratory Products Inc, USA). Bioreduced RABS were resuspended in anoxic 50 mM sodium bicarbonate to extract the U(VI) fraction that was unreacted and adsorbed. Non-crystalline and mineral-adsorbed U(IV) was extracted by an anoxic 1 M sodium bicarbonate solution at pH ~9. Lastly, the sediments were digested in aqua regia (3:1 mixture by volume of concentrated HCl and HNO_3) to determine the amount of recalcitrant crystalline U(IV) fraction (preseumed to correspond to UO_2). The extraction was repeated at least in triplicate so that the error of the assay is given as a standard deviation amongst the replicates. Aliquots of the digests were filtered through 0.22 µm PTFE filters (ThermoFisher, USA), diluted by an appropriate factor in 0.1 M nitric acid (HNO_3) and analyzed by ICP-MS for total U extracted from the solids.

Sulfur speciation

Sulfur XANES spectra (Figure S8) of the bottom layer from SRC2 are characterized by multiple oxidation states that were identified by comparing the energy position of the adsorption edges in model compounds used for the LCF analysis (Figure S2). The following oxidation states are clearly evident in the samples: S(-II) at 2,470.99-2,470.3 eV, S(0) at 2,472.2 eV and S(VI) at 2,482.6 eV. However, the dominant peak is positioned at 2,470.3 eV indicating that most of the S is present as S(-II). Thus, the best fits were obtained

including mackinawite that was exposed to sub-stoichiometric amounts of Fe(III). This FeS phase, referred as minimally oxidized mackinawite, exhibits a peak at 2470.3 eV, i.e., a peak shift in S XANES up to −0.6 eV compared to theoretical mackinawite[10] (Figure S2) (Table S3). The FeS model compound represents 91% of the total S in the system. The remaining fractions in S XANES are modeled by S(-I) as S associated with organics and a minor contribution of S(VI) (3%). Although the contribution of S(VI) in the fits is lower than the accuracy of the technique as reported in the literature (10%), it is considered as a relevant species as the peak is clearly distinguished in the spectra as discussed by Prietzel et *al.*[11].

Scanning transmission electron microscocopy

Samples were prepared by suspending the powder in ethanol by ultrasonication and drying a drop of the suspension on a carbon coated copper grid. STEM with energy dispersive spectroscopy (EDS) was used to obtain elemental composition maps and to perform comparative characterization of elemental content. In this study, an X-ray EDS system (Esprit/Quantax Bruker) in STEM mode in a FEI Tecnai Osiris microscope (200 kV X-FEG field emission gun, X-ray detector (Super-X) with 4 × 30 mm2 windowless SDD diodes and 0.9sr collection angle was applied. Quantitative EDS analysis was carried out using the Cliff-Lorimer standard-less method with thickness correction using K-series for all elements except uranium where M-series was used. The physical Bremsstrahlung background was calculated based on the sample composition. Some elements such as Cu contributing from the Cu grid were removed from quantification after the deconvolution procedure in the quantification process. Elemental concentrations in atomic % and net counts (signal above background) were derived from deconvoluted line intensities within a 95% confidence level. The process time and acquisition rates were adapted to get the most accurate data. A correction for specimen drift was applied during acquisition to improve elemental mapping accuracy.

Table S1 | Composition of Rifle artificial groundwater (RAGW)

Ion	mM
Ca^{2+}	4
K^{+}	0.3
Mg^{2+}	3.94
Na^{+}	7.52
Cl^{-}	2.7
HCO_3^{-}	1
SO_4^{2-}	14
pH	7.2

Table S2 | Total amount of uranium released from SRC2, SRC3, and SRC4 before the start of the U(VI) bioreduction phase (97 days) and at the end of the experiment (407 days).

column	U released during first 97 days		U released during all 407 days		RABS mass per column	Initial U content (prior to biostimulation) per column
	(µmoles)	(mg)	(µmoles)	(mg)	(kg)	(mg)
SRC2	7.5	1.8	8.2	1.9	0.5	2.5
SRC3	6.0	1.4	6.5	1.5	0.5	2.4
SRC4	5.5	1.3	5.8	1.4	0.5	2.5

Table S3 | Results of linear combination fit analysis of S K-edge XANES spectra of RABS bioreduced under sulfate-reducing conditions. The definition of R-factor and Chi-square are provided in SI Equation S1 and S2. Sulfur content was determined by XRF. Non-bolded values represent contributions that are below the quantifiable limit by LCF. Despite being below the 10% nominal cutoff for significance typically used for LCF, the contributions of sulfate and organic S are significant, as evidenced in Figure S8. * from Noel et al., 2017

	SRC2	
model compounds	**(%)**	**(wt. %)**
1. Mackinawite*	**91 ±1**	2.46
2. Elemental sulfur	1 ± 0.6	0.03
3. S in organics	**5 ± 1**	0.13
4. Sulfate	**3 ± 1**	0.08
sum		2.7
R-factor		0.0184
Chi-square		1.9053
Reduced chi-square		0.0052
Sulfur content (wt. %)		2.7

Table S4 | Results of linear combination fit analysis of Fe K-edge EXAFS and XANES spectra of RABS and SRC. The data, fits and weighted components are reported in Figure S10 (EXAFS) and Figure S20 (XANES). The definition of R-factor and Chi-square are provided in Equations S1 and S2. Non-bolded values represent contributions that are below the 10% cut-off for LCF and represent contributions that is not quantifiable by LCF.

	RABS		**SRC**	
	EXAFS	XANES	EXAFS	XANES
model compounds	(%)		(%)	
1. Illite	**22 ± 1**	**34 ± 2**	**52 ± 3**	**41 ± 5**
2. Biotite	**23 ± 1**	**16 ± 1**	**19 ± 2**	**28 ± 3**
3. Goethite	**33 ± 2**	**23 ± 2**	4 ± 4	8 ± 1
4. Hematite	**20 ± 1**	**25 ± 2**	0 ± 1	2 ± 1
5. Mackinawite	2 ± 2	2 ± 1	**25 ± 2**	**20 ± 2**
R-factor (%)	1.53	1.65E-04	2.08	2.96E-04
Fe content (wt. %)	4.83		5.5	

Table S5 | Results of linear combination fit analysis of U LIII edge XANES spectra of SRC2 and SRC4. The definitions of R-factor and Chi-square are provided in SI Equation 1 and 2. Non bolded values represent contributions that are below the 10% cut-off for LCF and represent contributions that is not quantifiable by LCF.

	SRC2		**SRC4**	
model compounds	**(%)**	**(ppm)**	**(%)**	**(ppm)**
1. U(IV) - NCU4	**86 ± 2**	404.37	**97 ± 2**	454.02
2. U(VI) - Uranyl adsorbed on ferrihydrite	**14 ± 1**	66.63	3 ± 1	14.98
sum		471		469
R-factor		0.0005		0.0032
Chi-square		0.0282		0.1272
Reduced chi-square		0.0002		0.0009
content of Uranium (ppm)		471		469

Table S6 | Results of the quantitative separation of U in the sediment.

	U(VI)		**NCU4**		**UO_2**	
	(%)	s.d.	(%)	s.d.	(%)	s.d.
SRC2	21%	1	70%	3	11%	5
SRC4	17%	1	75%	3	8%	5
SRC5	19%	2	70%	2	10%	5

Table S7 | Results of shell-by-shell fitting procedure of U L_{III} edge EXAFS spectra of the 12-month aged sample at 1 or 10 mM $NaHCO_3$ RAGW with and without the U-U shell, data and fits are plotted in Figure S13.

		1 mM $NaHCO_3$				10 mM $NaHCO_3$			
		without U-U		with U-U		without U-U		with U-U	
shell		fit	± error	fit	± error	fit	± error	fit	± error
$U\text{-}O_{ax}$	N	0.2	±0.1	0.2	±0.1	0.2	±0.1	0.3	±0.1
	R, Å	1.73	±0.04	1.74	±0.04	1.76	±0.03	1.72	±0.03
	σ^2, Å^2	0.003		0.003		0.003		0.003	
U-O	N	10.4	±1.6	10.1	±1.6	9.9	±1.3	9.8	±1.3
	R, Å	2.35	±0.01	2.38	±0.01	2.33	±0.01	2.38	±0.01
	σ^2, Å^2	0.016	±0.002	0.015	±0.002	0.016	±0.002	0.015	±0.002
$U\text{-}P_1$	N	2.1	±0.7	2.1	±0.4	1.9	±0.6	1.7	±0.6
	R, Å	3.11	±0.02	3.64	±0.02	3.11	±0.01	3.11	±0.01
	σ^2, Å^2	0.011	-	0.011	-	0.011	-	0.011	-
$U\text{-}P_2$	N	4.0	±0.4	3.8	±0.6	3.9	±0.3	3.9	±0.4
	R, Å	3.65	±0.03	3.14	±0.02	3.63	±0.02	3.63	±0.03
	σ^2, Å^2	0.011	-	0.011	-	0.011	-	0.011	-
U-U	N			0.5	±0.4			0.6	±0.5
	R, Å			3.88	-			3.87	-
	σ^2, Å^2			0.011	-			0.011	-
ΔE_0		3.3	±1.54	2.99	1.66	3.23	±1.31	3.2	±1.34
Red. Chi. Sqr.		51.9		57.3		14.1		15.9	
R factor		8.76E-03		7.44E-03		5.64E-03		4.56E-03	

Note: EXAFS fitting parameters include coordination number (N), interatomic distances (R(Å)), Debye Waller factor (σ^2(Å)) and energy shift ΔE_0 (eV). (-) fixed parameter; σ^2 of $U\text{-}O_{ax}$ is set based on the value reported by Kelly et *al.*2010[12], σ^2 of U-P1 and U-P2 are set based on the values reported by Alessi et *al.*2014[13], σ^2 of U-U is set based on the value reported by Kelly et *al.*2008[14]. Each model contain three MS paths for the U-O moiety MS1: $U\text{-}O_1\text{-}O_2\text{-}U$; MS2:$U\text{-}O_1\text{-}U\text{-}O_1$; MS3:$U\text{-}O_1\text{-}U\text{-}O_2$. The accuracy of the fits is evaluated by R_f as defined in SI Equation S1.

Table S8 | NCU4 in SRC2 sediments (aged 12 months in 10 mM NaHCO3); comparison of shell-by-shell fits for three scenarios with the corresponding continuous Cauchy-Wavelet Transform (CCWT) analysis being presented in Figure S14.

12 months aged NCU(IV) at 10 mM $NaHCO_3$							
		Scenario no. 1 C@2.9Å, P@3.6Å		Scenario no. 2 P@3.1Å, P@3.6Å		Scenario no. 3 Si@3.1Å, P@3.6Å	
shell		**fit**	**± error**	**fit**	**± error**	**fit**	**± error**
U-O_{ax}	**N**	0.2	±0.2	0.2	±±0.1	0.3	±0.1
	R	1.66	±0.05	1.76	±±0.03	1.71	±0.02
	σ^2	0.003	-	0.003	-	0.003	-
U-O	**N**	9.1	2.8	9.9	±1.3	9.8	1.2
	R	2.33	±0.02	2.33	±0.01	2.35	±0.01
	σ^2	0.016	±0.004	0.016	±0.002	0.016	±0.002
U-C	**N**	6.5	1.7				
	R	2.87	±0.03				
	σ^2	0.011	-				
U-P (@3.1Å)	**N**			1.9	±0.6		
	R			3.11	±0.01		
	σ^2			0.011	-		
U-Si	**N**					2.6	±0.2
	R					3.07	±0.02
	σ^2					0.005	-
U-P (@3.6Å)	**N**	3.8	±0.8	3.9	±0.3	3.3	±0.6
	R	3.54	±0.02	3.63	±0.02	3.6	±0.02
	σ^2	0.011	-	0.011	-	0.011	-
ΔE_0		3.05	2.96	3.23	1.31	1.71	1.08
Red. Chi. Sqr.		28.6		14.1		12.4	
R factor		1.15E-02		5.64E-03		4.97E-03	

Note: EXAFS fitting parameters include coordination number (N), interatomic distances (R(Å)), Debye Waller factor (σ^2(Å)) and energy shift ΔE_0 (eV). (-) fixed parameter; σ^2 of U-O_{ax} is set based on the value reported by Kelly et *al.*2010[12], σ^2 of U-P1 and U-P2 are set based on the values reported by Alessi et *al.*2014[13], σ^2 of U-C is set based on the value reported by Kelly et *al.*2010[14], σ^2 of U-Si is set based on the value reported by Labs et *al.*2014[15]. Each model contains three MS paths for the U-O moiety MS1: U-O_1-O_2-U; MS2: U-O_1-U- O_1 ; MS3:U-O_1-U-O_2. The accuracy of the fits is evaluated by R_f as defined in SI Equation S1.

Table S9 | Results of linear combination fit analysis of U LIII edge XANES spectra of the initial sediment (SRC2) and aged sediment at 1 mM and 10 mM bicarbonate concentration. The XANES LCF components are bioreduced non-crystalline U(IV) (NCU(IV)) and uranyl adsorbed on ferrihydrite (Figure S12). XANES LCF parameters are given in percentage of the total uranium in the sample. R-factor is defined as in Equation S1. Non-bolded values represent contributions that are below the 10% cut-off for LCF and are not quantifiable by LCF.

	U(VI)[a]	U(IV)[b]	R_f
	(%)	(%)	(10^{-3})
initial	**14 ± 2**	**86 ± 1**	0.5
4 mo. 1 mM HCO3	4 ± 1	**96 ± 1**	2.1
8 mo. 1 mM HCO3	2 ± 1	**98 (<1)**	7.8
12 mo. 1 mM HCO3	2 (<1)	**98 (<1)**	1.7
4 mo. 10 mM HCO3	3 (<1)	**97 ± 1**	3.9
8 mo. 10 mM HCO3	3 (<1)	**97 ± 1**	5.3
12 mo. 10 mM HCO3	3 (<1)	**97 (1)**	2.9

Table S10 | EDS measurements of biostimulated sediments after aging for a period of 12 months in RAGW at 1 mM HCO3 corresponding to images in Figures S15 and S16. Representative EDS spectra are reported in Figure S21.

Spectrum [at. %]	O	Mg	Al	Si	P	S	K	Ca	Ti	V	Mn	Fe	Ni	Cu	Zr	Pb	U
Figure S15 Area A	59.10	1.75	6.10	16.09	1.99	3.36	1.52	4.07	0.04	0.10	0.01	5.00	0.07	0.00	0.00	0.00	0.80
Figure S15 Area B	56.04	0.94	4.75	22.83	0.51	6.47	0.12	1.63	0.39	0.10	0.03	6.14	0.03	0.00	0.00	0.00	0.02
Figure S16	60.53	0.64	0.92	6.15	0.21	1.92	0.00	2.08	0.29	0.06	0.17	23.90	0.32	0.00	0.00	0.00	2.81

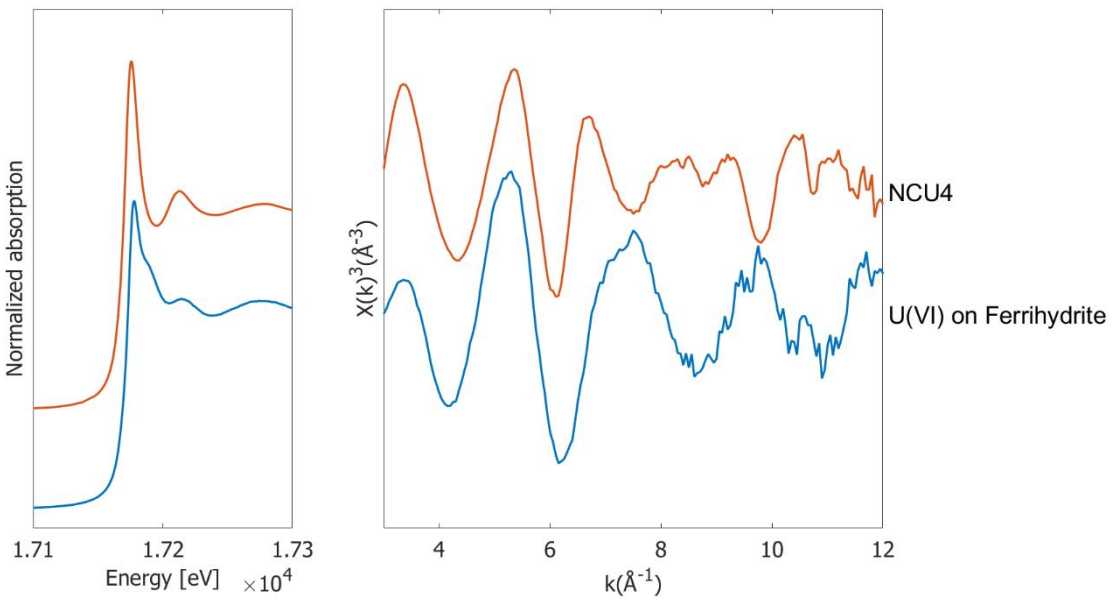

Figure S1 | XANES (left) and EXAFS (right) spectra of reference compounds used for linear combination fit analysis of U K-edge

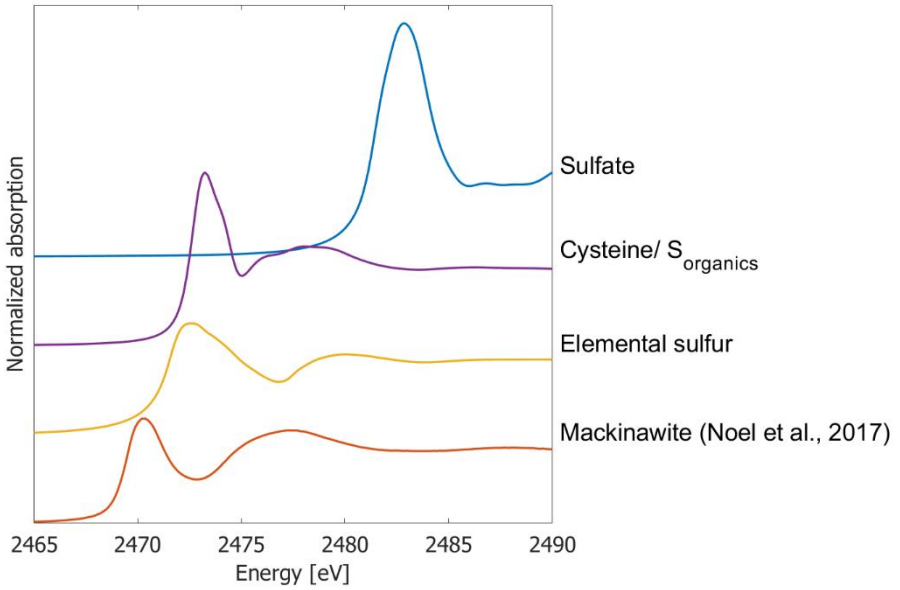

Figure S2 | XANES spectra of reference compounds utilized for linear combination fit analysis of S K-edge XANES

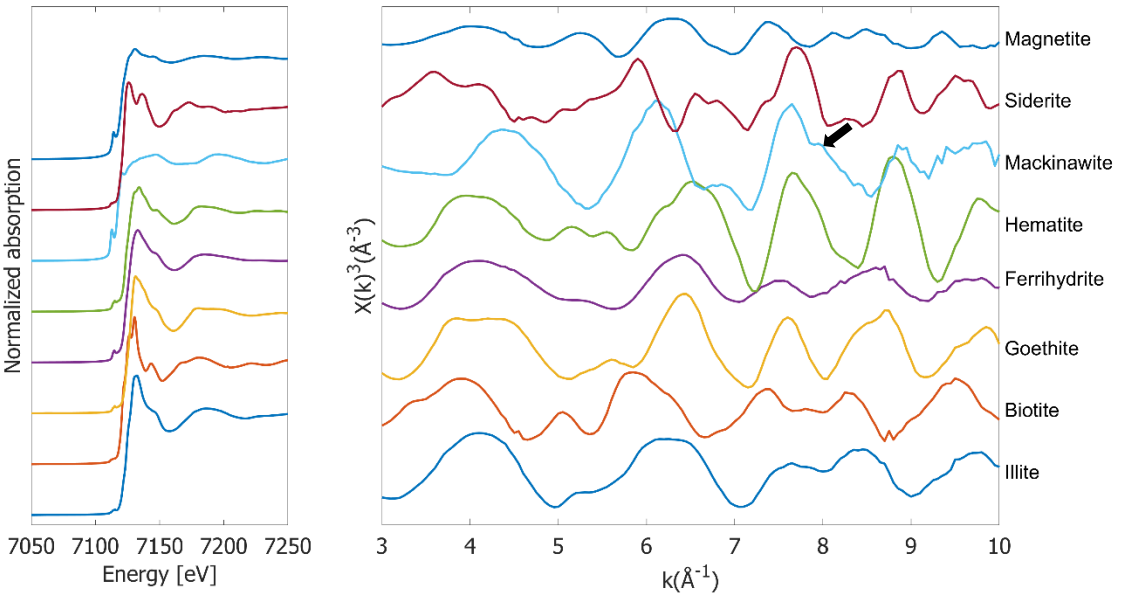

Figure S3 | XANES (left) and EXAFS (right) spectra of reference compounds used for linear combination fit analysis of Fe K-edge. The arrow indicates the feature at 8 Å that is characteristic of mackinawite.

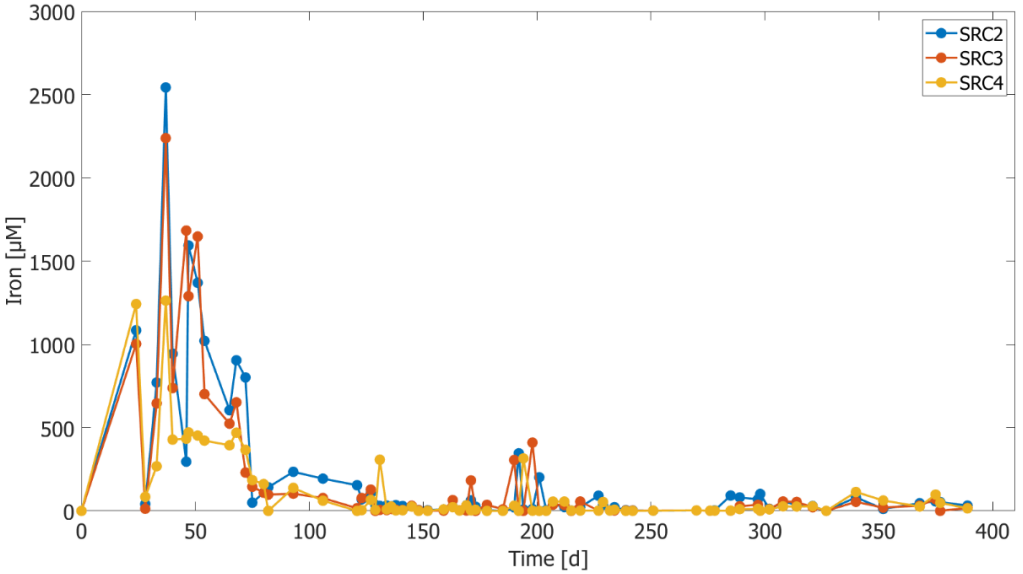

Figure S4 | Total iron concentration in the effluents of SRC2, SRC3, SRC4 over time.

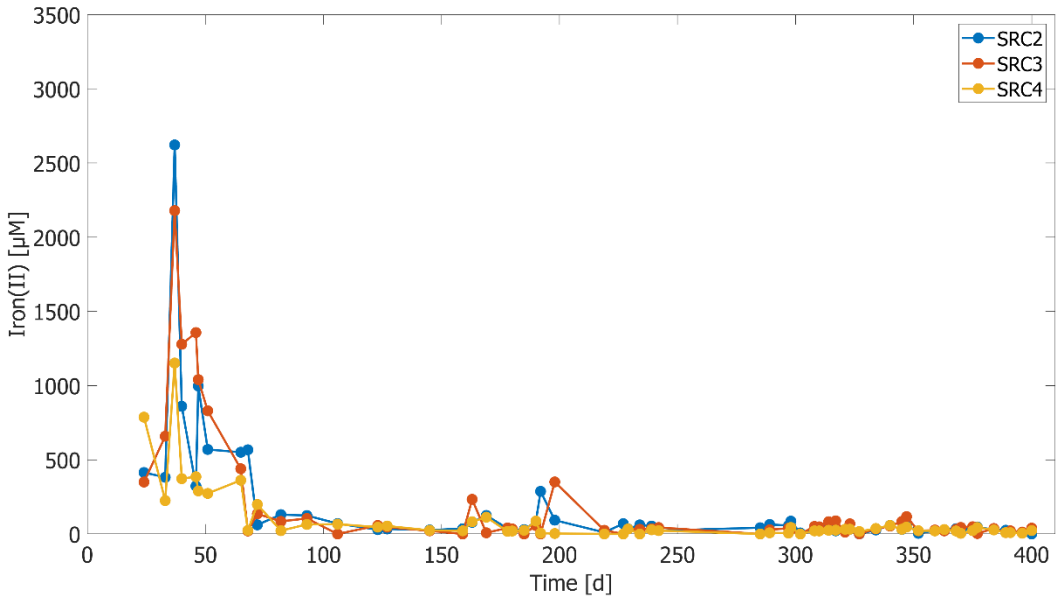

Figure S5 | Iron(II) concentration in the effluents of SRC2, SRC3, SRC4 over time.

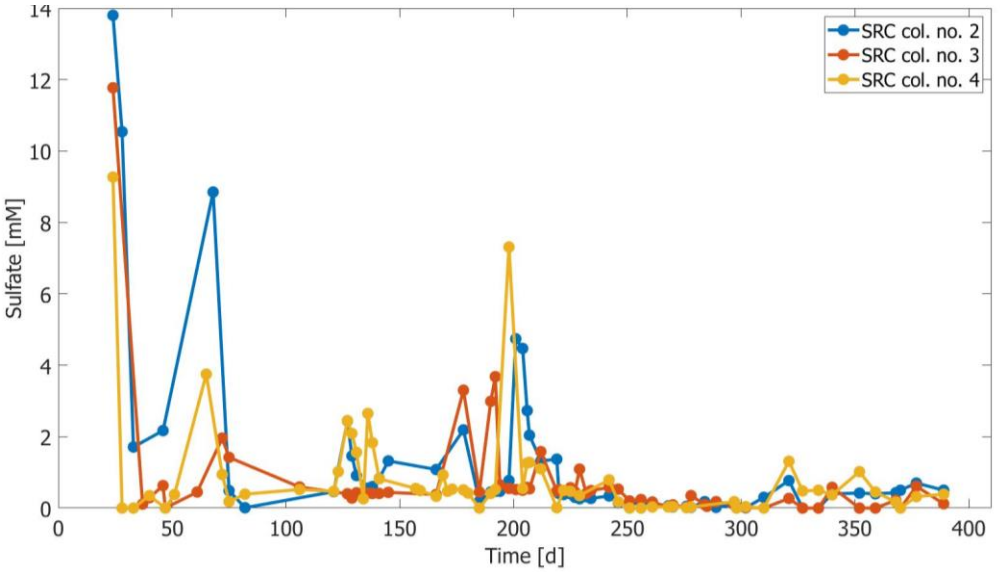

Figure S6 | Sulfate concentration in the effluents of SRC2, SRC3, SRC4 over time.

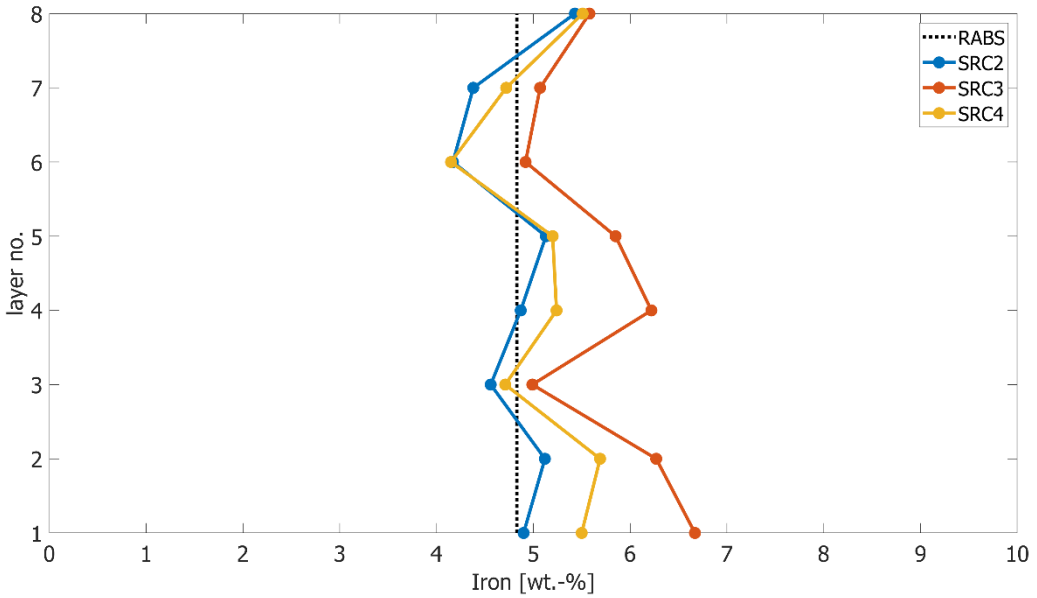

Figure S7 | XRF measurements of the iron content per layer in SRC and IRC columns. The sediments in columns after bioreduction were retrieved by slicing the entire column into layers of equal thickness (~2cm). Hence, the layer no. in the y-axis indicates the layer of sediment in the column. Layer 1 is at the bottom of the column and layer 8 at the top. The dotted line represents the average concentration of Fe in RABS.

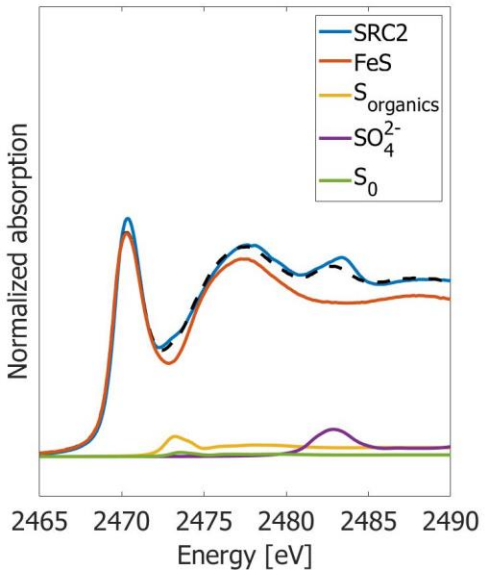

Figure S8 | S K-edge XANES data and fit (black dashed line) and the weighted contribution of the compounds required for the LCF fit of SRC sediments from column 2 (SRC2). The sediments for XAS speciation were sampled from the bottom layer (layer no. 1 in Figures S7, S9 and S11) of the column at the end of the bioreduction phase.

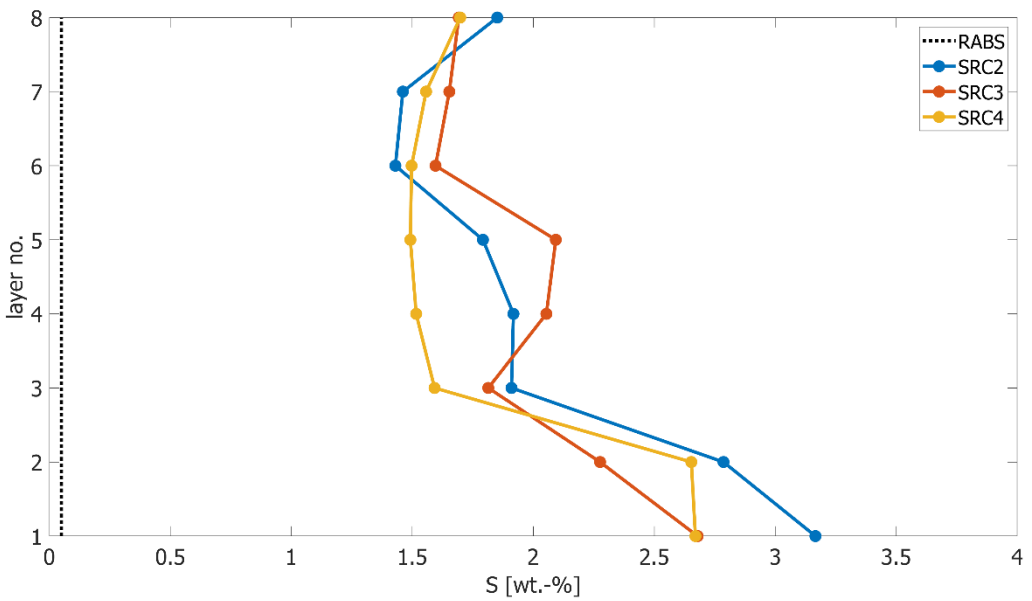

Figure S9 | XRF measurements of the sulfur content per layer in SRC columns. The sediments in columns after bioreduction were retrieved by slicing the entire column into layers of equal thickness (~2cm). Hence, the layer no. in the y-axis indicates the layer of sediment in the column. Layer 1 is at the bottom of the column and layer 8 at the top. The dotted line on the left-hand side represents the concentration of S in RABS.

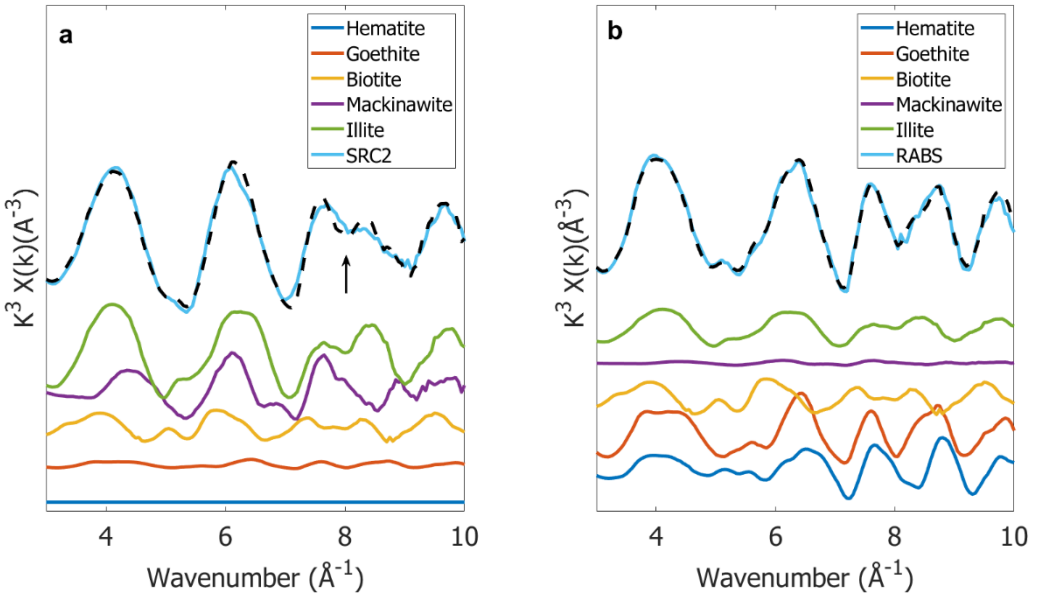

Figure S10 | Fe K-edge EXAFS data (blue) and fit (black dashed line) and the weighted contribution of the compounds used for the LCF for (a) SRC sediments from column 2 and (b) pristine RABS sediments. The vertical black arrow in panel a points at the distinctive feature at 8 Å that is typically attributed to mackinawite. The sediments for XAS speciation were sampled from the bottom layer (layer no. 1 in Figures S7, S9 and S11) of the column at the end of the bioreduction phase.

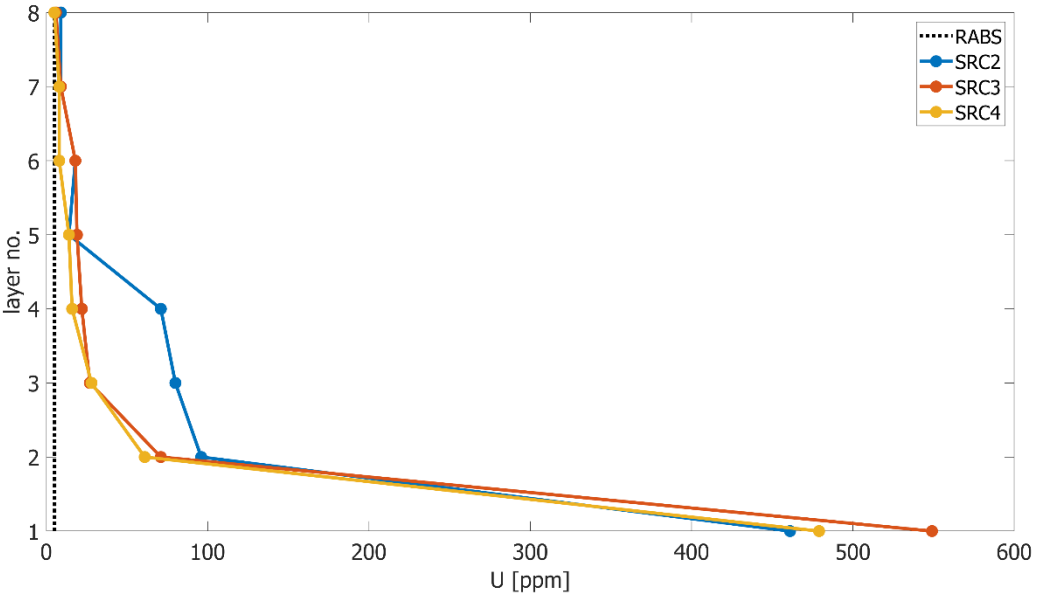

Figure S11 | XRF measurements of the uranium content per layer in SRC column 2, 3 and 4 (SRC2, SRC3, SRC4). The sediments in columns after bioreduction were retrieved by slicing the entire column into layers of equal thickness (~2cm). Hence, the layer no. in the y-axis indicates the layer of sediment in the column. Layer 1 is at the bottom of the column and layer 8 at the top. The dotted line on the left-hand side represents the concentration of U in RABS.

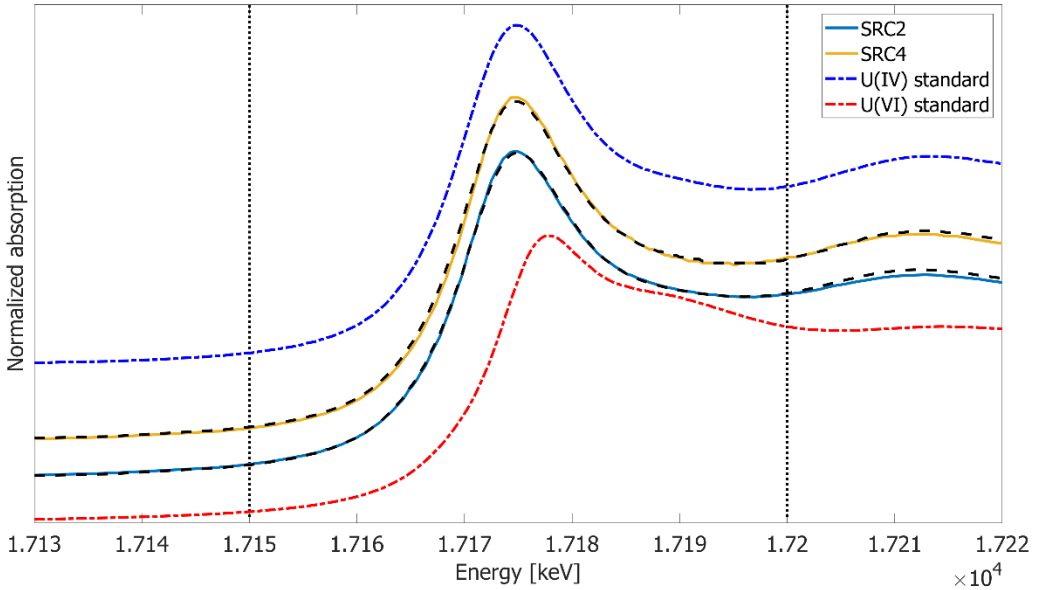

Figure S12 | Uranium LIII-edge XANES of the SRC2 and SRC4 bioreduced under sulfate-reducing conditions. The sediments for XAS speciation were sampled from the bottom layer (layer no. 1 in Figures S7, S9 and S11) of the column at the end of the bioreduction phase.

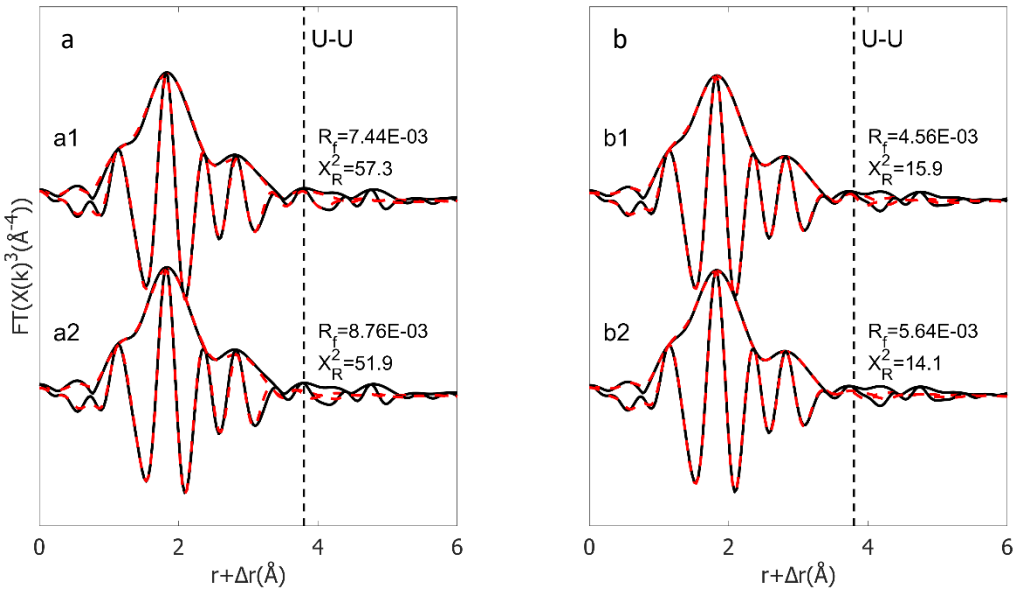

Figure S13 | Result of shell-by-shell fit analysis of 12-month aged samples at (a) low bicarbonate and (b) high bicarbonate. Fits a1 and b1 contains the contribution of U-U path with CN 0.5 in a1 and 0.6 in b1 and fits a2 and b2 do not. The goodness of the fits is evaluated on the R-factor (Rf) and the Reduced Chi-squared (X2r) as defined in Equations S1 and S2. Corresponding fit parameters are reported in Table S7. The sediments for XAS speciation were sampled from the bottom layer (layer no. 1 in Figure S7, S9 and S11) of the column at the end of the bioreduction phase.

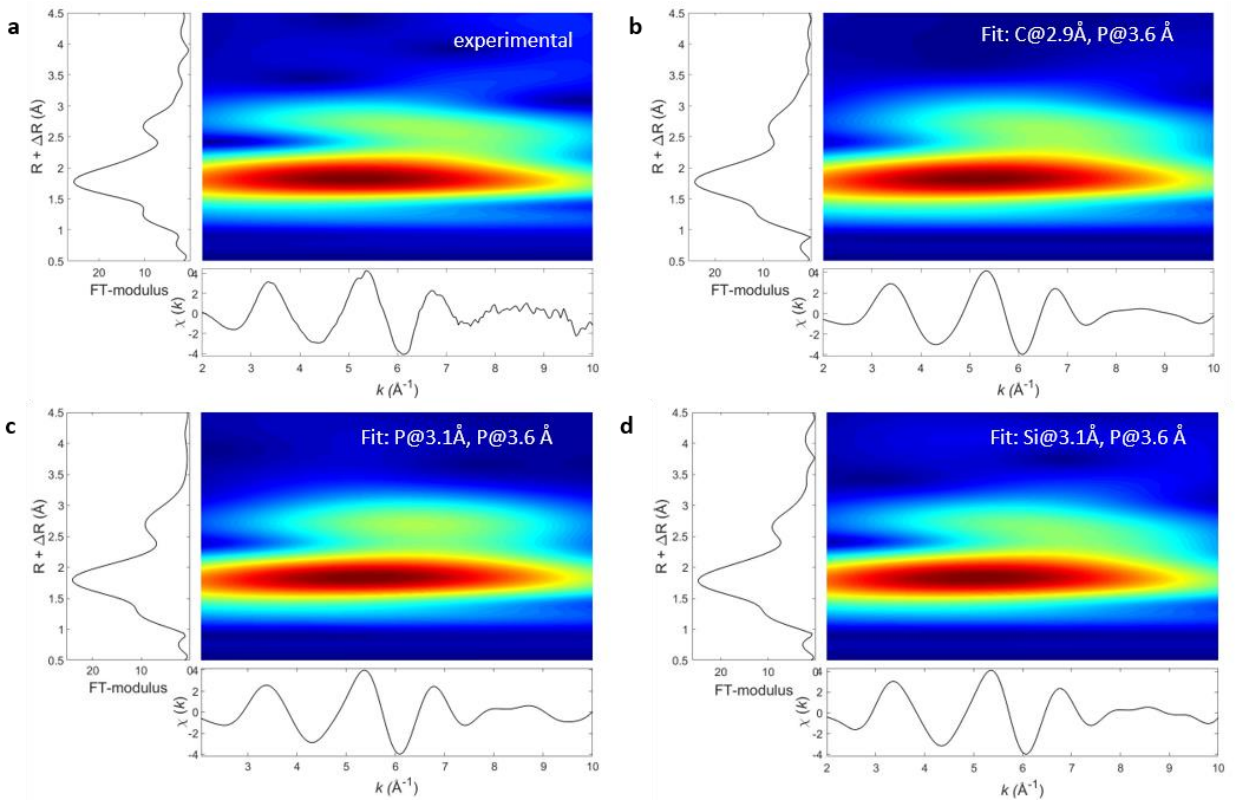

Figure S14 | Comparison of Continuous Cauchy-Wavelet transform (CCWT) of U LIII-edge EXAFS of (a) experimental data and (b) calculated EXAFS with bidentate C and monodentate P or (c) bidentate P and monodentate P or (d) bidentate Si and monodentate P. The color code corresponds to the intensity of the EXAFS signal in arbitrary units from blue to red. The ordinate axis corresponds to the distance R+ΔR (Å) from the absorber. Corresponding fit parameters are reported in Table S8. The sample is SRC2 aged 12 months in 10 mM NaHCO3.

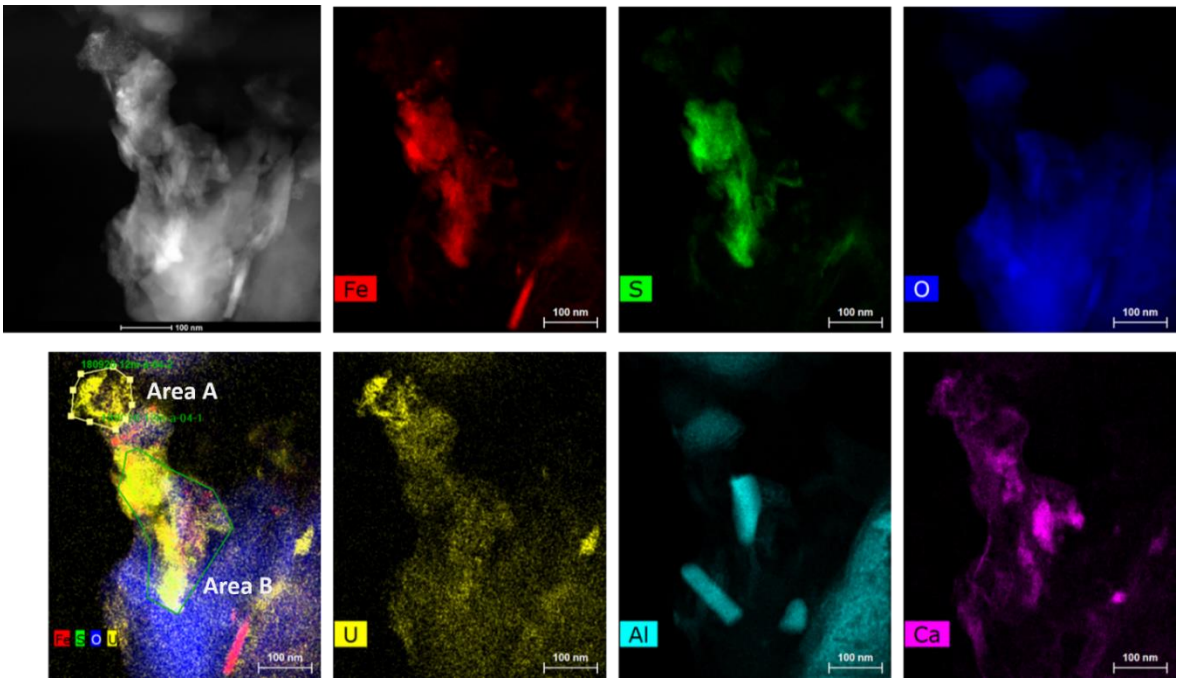

Figure S15 | STEM image of bioreduced sediment after 12 months aging in RAGW at 1 mM HCO3. Corresponding EDS data for the area A and B are presented in Table S10. U is present both as discrete precipitates and as a diffuse species on the surface of an FeS and clay particle aggregate.

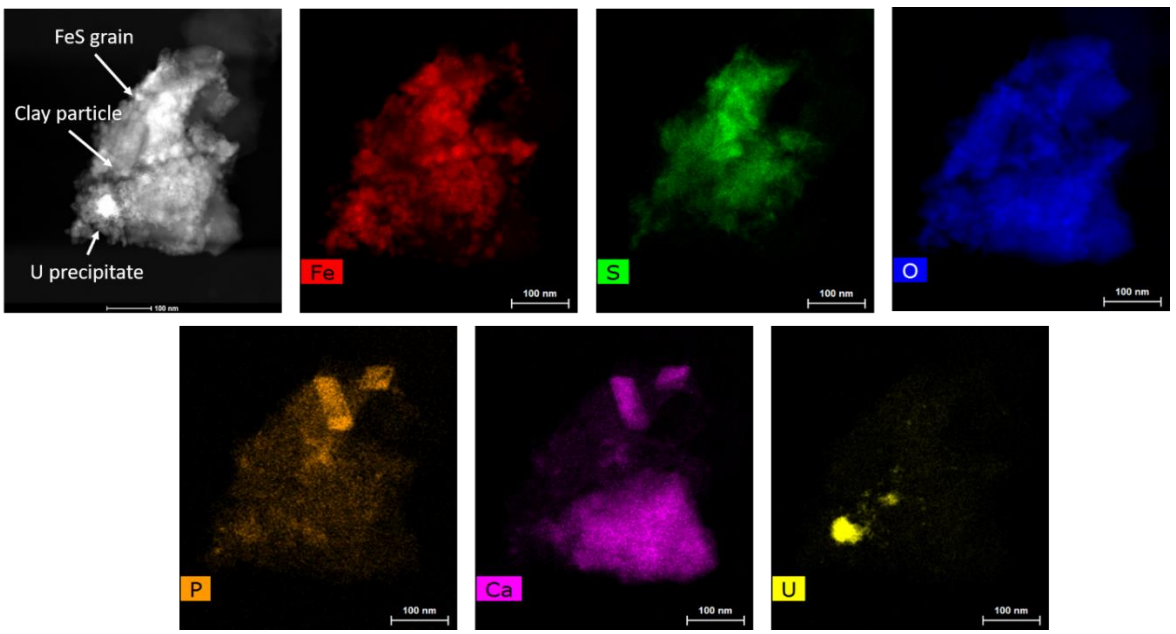

Figure S16 | STEM image of bioreduced sediment after 12 months aging in RAGW at 1 mM HCO3. Corresponding EDS data are presented in Table S10. U is present as a discrete precipitate in association with an FeS grain and a clay particle aggregate.

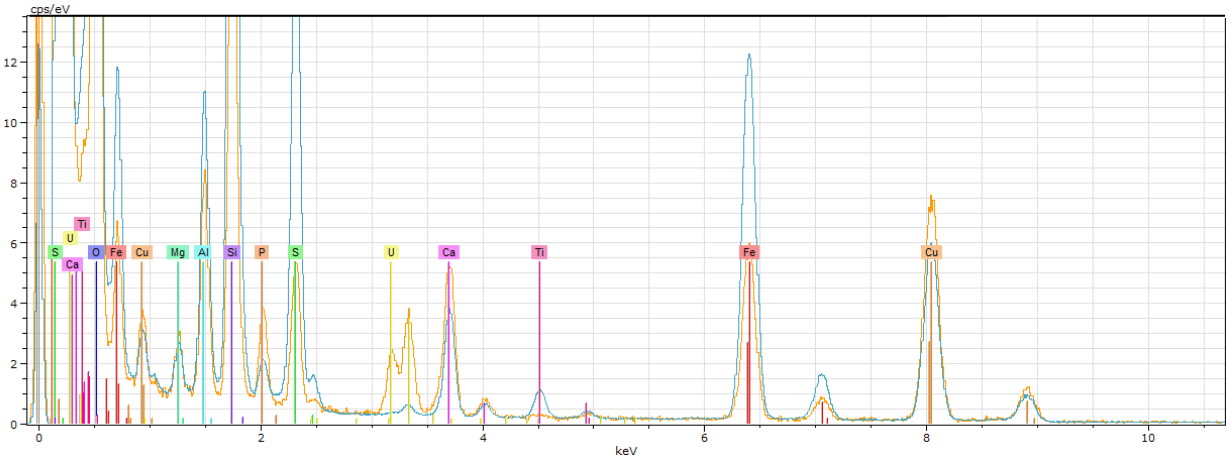

Figure S17 | EDS spectra of area A (yellow) and area B (blue) in Figure S15.

$$\boldsymbol{R\_factor} = \sum(\boldsymbol{X(k)}_{\boldsymbol{experimental\ data}} - \boldsymbol{X(k)}_{\boldsymbol{fit}})^2 \Big/ \sum(\boldsymbol{X}_{\boldsymbol{experimental\ data}})^2$$

Equation S1 definition of R-factor

$$X_r^2 = \frac{N_{ind}}{vn} \sum_{i=1}^{n} \frac{(k^3 X(k)_{experimental\ data,i} - k^3 X(k)_{fit,i})^2}{\varepsilon_i^2}$$

Equation S2 Definition of reduced Chi-square X_r^2

With N_{ind} is the number of independent variables, v is the degree of freedom, n is the number of fitted data points, and ε is the measurement uncertainty for each data point.

References

(1) Anderson, R. T.; Vrionis, H. A.; Ortiz-Bernad, I.; Resch, C. T.; Long, P. E.; Dayvault, R.; Karp, K.; Marutzky, S.; Metzler, D. R.; Peacock, A.; et al. Stimulating the In Situ Activity of Geobacter Species To Remove Uranium from the Groundwater of a Uranium-Contaminated Aquifer. *Appl. Environ. Microbiol.* **2003**, *69* (10), 5884–5891. https://doi.org/10.1128/AEM.69.10.5884-5891.2003.

(2) Komlos, J.; Peacock, A.; Kukkadapu, R. K.; Jaffé, P. R. Long-Term Dynamics of Uranium Reduction/Reoxidation under Low Sulfate Conditions. *Geochimica et Cosmochimica Acta* **2008**, *72* (15), 3603–3615. https://doi.org/10.1016/j.gca.2008.05.040.

(3) Yabusaki, S. B.; Fang, Y.; Long, P. E.; Resch, C. T.; Peacock, A. D.; Komlos, J.; Jaffe, P. R.; Morrison, S. J.; Dayvault, R. D.; White, D. C.; et al. Uranium Removal from Groundwater via in Situ Biostimulation: Field-Scale Modeling of Transport and Biological Processes. *J. Contam. Hydrol.* **2007**, *93* (1–4), 216–235. https://doi.org/10.1016/j.jconhyd.2007.02.005.

(4) Moon, H. S.; Komlos, J.; Jaffé, P. R. Uranium Reoxidation in Previously Bioreduced Sediment by Dissolved Oxygen and Nitrate. *Environ. Sci. Technol.* **2007**, *41* (13), 4587–4592. https://doi.org/10.1021/es063063b.

(5) Campbell, K. M.; Kukkadapu, R. K.; Qafoku, N. P.; Peacock, A. D.; Lesher, E.; Williams, K. H.; Bargar, J. R.; Wilkins, M. J.; Figueroa, L.; Ranville, J.; et al. Geochemical, Mineralogical and Microbiological Characteristics of Sediment from a Naturally Reduced Zone in a Uranium-Contaminated Aquifer. *Applied Geochemistry* **2012**, *27* (8), 1499–1511. https://doi.org/10.1016/j.apgeochem.2012.04.013.

(6) Moon, H. S.; McGuinness, L.; Kukkadapu, R. K.; Peacock, A. D.; Komlos, J.; Kerkhof, L. J.; Long, P. E.; Jaffé, P. R. Microbial Reduction of Uranium under Iron- and Sulfate-Reducing Conditions: Effect of Amended Goethite on Microbial Community Composition and Dynamics. *Water Research* **2010**, *44* (14), 4015–4028. https://doi.org/10.1016/j.watres.2010.05.003.

(7) Mehta, V. S.; Maillot, F.; Wang, Z.; Catalano, J. G.; Giammar, D. E. Transport of U(VI) through Sediments Amended with Phosphate to Induce in Situ Uranium Immobilization. *Water Research* **2015**, *69* (Supplement C), 307–317. https://doi.org/10.1016/j.watres.2014.11.044.

(8) Stookey, L. L. Ferrozine---a New Spectrophotometric Reagent for Iron. *Anal. Chem.* **1970**, *42* (7), 779–781. https://doi.org/10.1021/ac60289a016.

(9) Alessi, D. S.; Uster, B.; Veeramani, H.; Suvorova, E. I.; Lezama-Pacheco, J. S.; Stubbs, J. E.; Bargar, J. R.; Bernier-Latmani, R. Quantitative Separation of Monomeric U(IV) from UO2 in Products of U(VI) Reduction. *Environ. Sci. Technol.* **2012**, *46* (11), 6150–6157. https://doi.org/10.1021/es204123z.

(10) Noël, V.; Boye, K.; Kukkadapu, R. K.; Bone, S.; Lezama Pacheco, J. S.; Cardarelli, E.; Janot, N.; Fendorf, S.; Williams, K. H.; Bargar, J. R. Understanding Controls on Redox Processes in Floodplain Sediments of the Upper Colorado River Basin. *Science of The Total Environment* **2017**, *603–604*, 663–675. https://doi.org/10.1016/j.scitotenv.2017.01.109.

(11) Prietzel, J.; Botzaki, A.; Tyufekchieva, N.; Brettholle, M.; Thieme, J.; Klysubun, W. Sulfur Speciation in Soil by S K-Edge XANES Spectroscopy: Comparison of Spectral Deconvolution and Linear Combination Fitting. *Environ. Sci. Technol.* **2011**, *45* (7), 2878–2886. https://doi.org/10.1021/es102180a.

(12) Kelly, S. D.; Wu, W.-M.; Yang, F.; Criddle, C. S.; Marsh, T. L.; O'Loughlin, E. J.; Ravel, B.; Watson, D.; Jardine, P. M.; Kemner, K. M. Uranium Transformations in Static Microcosms. *Environ. Sci. Technol.* **2010**, *44* (1), 236–242. https://doi.org/10.1021/es902191s.

(13) Alessi, D. S.; Lezama-Pacheco, J. S.; Janot, N.; Suvorova, E. I.; Cerrato, J. M.; Giammar, D. E.; Davis, J. A.; Fox, P. M.; Williams, K. H.; Long, P. E.; et al. Speciation and Reactivity of Uranium Products Formed during in Situ Bioremediation in a Shallow Alluvial Aquifer. *Environ. Sci. Technol.* **2014**, *48* (21), 12842–12850. https://doi.org/10.1021/es502701u.

(14) Kelly, S. D.; Kemner, K. M.; Carley, J.; Criddle, C.; Jardine, P. M.; Marsh, T. L.; Phillips, D.; Watson, D.; Wu, W.-M. Speciation of Uranium in Sediments before and after In Situ Biostimulation. *Environ. Sci. Technol.* **2008**, *42* (5), 1558–1564. https://doi.org/10.1021/es071764i.

(15) Labs, S.; Hennig, C.; Weiss, S.; Curtius, H.; Zänker, H.; Bosbach, D. Synthesis of Coffinite, $USiO_4$, and Structural Investigations of $U_x Th_{(1-x)} SiO_4$ Solid Solutions. *Environmental Science & Technology* **2014**, *48* (1), 854–860. https://doi.org/10.1021/es403995b.